Supplementary Information for:

Interface Engineering of the Photoelectrochemical Performance of Ni-Oxide-Coated n-Si Photoanodes by Atomic-Layer Deposition of Ultrathin Films of Cobalt Oxide

Xinghao Zhou[1,2]†, Rui Liu[1]†, Ke Sun[1,3]†, Dennis Friedrich[1,4], Matthew T. McDowell[1,3], Fan Yang[1,3], Stefan T. Omelchenko[1,2], Fadl H. Saadi[1,2], Adam C. Nielander[3], Sisir Yalamanchili[1,2], Kimberly M. Papadantonakis[1,3], Bruce S. Brunschwig[1,5], Nathan S. Lewis[1,3,5,6*]

[1]Joint Center for Artificial Photosynthesis, California Institute of Technology, Pasadena, CA 91125, USA

[2]Division of Materials Science, California Institute of Technology, Pasadena, CA 91125, USA

[3]Division of Chemistry and Chemical Engineering, California Institute of Technology, Pasadena, CA 91125, USA

[4]Institute for Solar Fuels, Helmholtz-Zentrum Berlin für Materialien und Energie, Hahn-Meitner Platz 1, 14109 Berlin, Germany

[5]Beckman Institute and Molecular Materials Research Center, California Institute of Technology, Pasadena, CA 91125, USA

[6]Kavli Nanoscience Institute, California Institute of Technology, Pasadena, CA 91125, USA

† These authors contributed equally

*Corresponding author: nslewis@caltech.edu

Experimental Details:

Chemicals:

All materials were used as received unless noted otherwise: Potassium hydroxide pellets (KOH, Macron Chemicals, ACS 88%), buffered HF improved (Transene Company Inc.), concentrated hydrochloric acid (HCl, EMD, ACS Reagent grade, 36.5-38%), sulfuric acid (H_2SO_4, Mallinckrodt Chemicals, ACS Reagent grade, 95%-98%), hydrogen peroxide (H_2O_2, Macron Chemicals, ACS grade 30%), potassium chloride (KCl, Macron Chemicals, Granular ACS 99.6%), potassium ferrocyanide trihydrate ($K_4Fe(CN)_6 \bullet 3H_2O$, Acros, >99%), potassium ferricyanide ($K_3Fe(CN)_6$, Fisher Chemicals, certified ACS 99.4%), methanol (CH_3OH, low water content, J. T. Baker, 99.8%). Water with a resistivity $\geqslant$ 18 MΩ·cm was obtained from a Barnsted Nanopure deionized (DI) water system.

For non-aqueous electrochemistry, acetonitrile (CH_3CN, anhydrous, Sigma-Aldrich, 99.8%) was dried by flowing the solvent through a column of activated Al_2O_3, followed by storage over 3 Å activated molecular sieves (Sigma-Aldrich). Lithium perchlorate ($LiClO_4$, Sigma-Aldrich, battery grade 99.99%) was dried at 300 K under a pressure < 1×10^{-3} Torr. Bis(cyclopentadienyl) iron(II) (ferrocene, $FeCp_2$, Sigma-Aldrich), bis(pentamethylcyclopentadienyl)iron ($Me_{10}Cp_2Fe$, decamethyl ferrocene, Strem, 99%), bis(cyclopentadienyl)cobalt(II) (Cp_2Co, cobaltocene, Strem, 98%) and bis(methylcyclopentadienyl)iron (Me_2Cp_2Fe, 1,1'-dimethylferrocene, Sigma-Aldrich, 95%) were purified by sublimation under vacuum. Bis(cyclopentadienyl) iron(III) tetrafluoroborate (ferrocenium, $FeCp_2^+$ BF_4^-, Sigma Aldrich, technical grade), and bis(cyclopentadienyl)cobalt(III) hexafluorophosphate (Cobaltocenium hexafluorophosphate,

$CoCp_2^+PF_6^-$, Sigma-Aldrich, 98%) were recrystallized from diethyl ether (EMD, ACS grade) and CH_3CN (EMD Chemicals, ACS grade), and dried under vacuum. Bis(pentamethylcyclopentadienyl)ferrocenium tetrafluoroborate (decamethylferrocenium, $Me_{10}Fe^+BF_4^-$) and bis(methylcyclopentadienyl)iron tetrafluoroborate ($Me_2Cp_2Fe^+BF_4^-$) were synthesized by chemical oxidation of the neutral metallocenes.[1]

Preparation of substrates:

Phosphorus-doped (n-type, (100)-oriented, single-side polished, resistivity 0.1-1 ohm cm) and degenerately boron-doped (p^+-type, (100)-oriented, single-side polished, resistivity <0.005 ohm cm) Si wafers were purchased from Addison Engineering Inc. The n-Si wafers were first cleaned using a piranha etching procedure by soaking the wafers in a mixed solution of H_2SO_4 and H_2O_2 (3:1 by volume) for 10 min. The n-type wafers were then cleaned in a buffered HF etchant for 1 min, followed by etching the Si wafers using an RCA SC-2 procedure consisting of soaking the wafers in a solution of H_2O, concentrated hydrochloric acid and hydrogen peroxide (6:1:1 volume ratio) for 10 min at 75 °C. Finally, the n-type wafers were thoroughly rinsed using DI water and dried with a flow of N_2. This procedure left a thin layer of SiO_x ($SiO_{x,\ RCA}$) on the surface of the n-Si wafers. The p^+-Si wafers were etched by soaking the samples in a buffered HF oxide etchant for 1 min to remove the native oxide layer before sputter-deposition of NiO_x.

Atomic-layer deposition of transition metal oxides:

Atomic-layer deposition (ALD) of CoO_x was conducted at 150 °C using cobaltocene and ozone in

a Cambridge Nanotech S200 ALD system (all ALD processes were conducted in this system). The cobaltocene precursor was heated and maintained at 80 °C. An ALD cycle consisted of a 2 s pulse of the cobaltocene precursor, a 10 s purge under 20 cm^3 min^{-1} flow of research-grade N_2(g), a 5 s ozone pulse and another 10 s N_2 (g) purge.

ALD of FeO_x was conducted at 150 °C from ferrocene and ozone. The ferrocene was heated and maintained at 85 °C. An ALD cycle consisted of a 5 s pulse of the ferrocene precursor, a 15 s purge under a 20 cm^3 min^{-1} flow of research-grade N_2(g), a 5 s ozone pulse, and another 15 s N_2 (g) purge.

ALD of NiO_x was conducted at 150 °C using $Ni(ethylCp)_2$ and ozone. The $Ni(EtCp)_2$ precursor was heated and maintained at 60 °C. An ALD cycle consisted of a 0.5 s pulse of the $Ni(EtCp)_2$ precursor, a 4 s purge under a 20 cm^3 min^{-1} flow of research-grade N_2(g), a 7 s ozone pulse, and another 60 s N_2 (g) purge.

Sixty ALD cycles were used for all ALD transition-metal oxide coatings described in this work.

Sputter-deposition of NiO_x:

NiO_x was deposited via reactive RF sputtering from a Ni target (Kurt Lesker, 2'' diameter × 0.125'' thickness, 99.95%) using an AJA high-vacuum magnetron sputtering system (AJA International Inc.). The O_2 and Ar flows were kept at 1 sccm and 20 sccm, respectively, while the working pressure was held at 5 mTorr, with the substrates maintained at 300 °C. A deposition rate of 0.4 Å s^{-1} was maintained by tuning the sputtering power on the Ni target.

Sputtered NiO_x films deposited on semiconductor substrates have demonstrated

multiple desired functionalities simultaneously, including protection against corrosion, hole conduction, and inherent activity for the water-oxidation reaction. Moreover, tuning the physical thickness of the film to 75-85 nm (depending on the refractive index of the substrate) results in enhanced transparency of the film especially under water-oxidation conditions, negligible losses due to film resistivity, and antireflective properties which optimize absorption within the Si substrate.[2-4]

Preparation of electrodes:

The back sides of the Si samples were rubbed with an In-Ga alloy (Alfa Aesar, 99.99%) to form ohmic contacts. Ag paste was then used to attach the ohmic contact to a coiled, tin-plated Cu wire (McMaster-Carr) which was then threaded through a glass tube (Corning Inc., Pyrex tubing, 7740 glass). The samples were then encapsulated and sealed to the glass tube using grey epoxy (Hysol 9460F). The exposed electrode surfaces were imaged with a high-resolution optical scanner (Epson perfection V370 with a resolution of 2400 psi) and the areas were measured using ImageJ software. All of the electrodes were 0.1-0.2 cm^2 in area unless specified otherwise.

Aqueous and non-aqueous electrochemical measurements:

For electrochemical measurements in 1.0 M KOH(aq), including photoelectrochemical, spectral response and electrochemical impedance spectroscopy, a mercury/mercury oxide (Hg/HgO in 1.0 M KOH(aq), CH instruments, CH152) electrode was used as the reference electrode, and a carbon cloth in a fritted glass tube (gas dispersion tube Pro-D, Aceglass, Inc.) was used as the counter electrode. The Hg/HgO reference electrode had a potential of 0.926 V

versus the reversible hydrogen electrode, RHE. For electrochemical measurements performed in 50 mM $K_3Fe(CN)_6$, 350 mM $K_4Fe(CN)_6$ and 1.0 M KCl as well as for measurements in non-aqueous solutions, a Pt wire (0.5 mm diameter, 99.99% trace metal basis, Alfa, Aesar) was used as the reference electrode and a Pt gauze was used as the counter electrode. A custom electrochemical cell with a flat glass (Pyrex) bottom was used for all electrochemical measurements. During measurements, the electrolyte was vigorously agitated with a magnetic stir bar driven by a model-train motor (Pittman). A Xe arc lamp (Newport 67005 and 69911) equipped with an IR filter (Newport 61945) and with an AM 1.5 filter (Newport 81094 and 71260), as well as ELH-type (Sylvania/Osram) and ENH-type (EIKO) tungsten-halogen lamps with a custom housing with a transformer (Staco Energy Products Co.), were used for photoelectrochemical stability measurements. The illumination intensity was calibrated by placing a Si photodiode (FDS100-Cal, Thorlabs) in the cell, in the same position as the exposed area of the photoelectrode. Because all of the photoelectrodes were bottom-facing, a broadband reflection mirror (Newport dielectric mirror, 10Q20PR-HR) was used to direct the light beam from the horizontal to the vertical direction. For non-aqueous tests in methanol, the cell was assembled in an Ar-filled glove box, but photoelectrodes were measured outside the glove box while the cell was purged with Ar. All of the data presented for electrochemical measurements in aqueous solutions did not include compensation for the series resistance of the solution.

Cyclic voltammetry, quantum yield, and electrochemical impedance spectroscopy data were obtained using a Biologic SP-200 potentiostat (Bio-Logic Science Instruments). The stability test data were obtained using a Biologic MPG-2-44 potentiostat (Bio-Logic Science Instruments).

The cyclic voltammetric data was recorded at a constant rate of 40 mV s^{-1}. The external quantum yield data were collected with the potentiostat connected to a lock-in amplifier while scanning the wavelengths produced by a monochromated light source were chopped at a frequency of 20 Hz.

Electrochemical Impedance Spectroscopy and Mott-Schottky Analysis

Electrochemical impedance spectroscopy was performed in 50 mM $K_3Fe(CN)_6$, 350 mM $K_4Fe(CN)_6$ and 1.0 M KCl(aq). The solution was in the dark during the measurements. The electrochemical impedance data were fit to a model that consisted of a parallel resistor and a capacitor with a fixed constant-phase element at the Si interface arranged electrically in series with another resistor and capacitor in parallel at the NiO_x/electrolyte interface.

The reverse-bias dependence of the area-normalized differential capacitance in the depletion region of the semiconductor is given by the Mott-Schottky relation:

$$\frac{1}{C^2} = \frac{2}{A^2 \varepsilon_0 \varepsilon_r q N_d}\left(V_{app} - V_{fb} - \frac{k_B T}{q}\right)$$

where *A* is the device area, ε_0 is the vacuum permittivity, ε_r is the relative permittivity, *q* is the unsigned charge on an electron, N_d is the donor impurity concentration in the semiconductor, V_app is the difference between the applied potential and the redox potential of the solution, V_fb is the flat-band potential, k_B is Boltzmann's constant, and *T* is the temperature in K. Mott-Schottky plots were linear ($R^2 > 0.999$).

The doping density was calculated using:

$$N_d = \frac{2}{A^2 q \varepsilon_0 \varepsilon_r \left[\frac{d\left(\frac{1}{C^2}\right)}{dV_{app}}\right]}$$

Electrochemistry under different light intensities and effective Richardson constant calculation:

Neutral density filters with an optical density (OD) of either 0.2, 0.4, 0.6, 0.8, 1.0 were used to attenuate the intensity of light when performing electrochemistry under 1 Sun for the n-Si/$SiO_{x,RCA}$/CoO_x/NiO_x electrode in a solution of 50 mM $K_3Fe(CN)_6$, 350 mM $K_4Fe(CN)_6$ and 1.0 M KCl(aq).

The *J-V* characteristic of an n-Si/$SiO_{x,RCA}$/CoO_x/NiO_x electrode in the dark can be expressed as:

$$J = J_{01}\left(Exp\left(\frac{qV}{n_1 k_B T}\right) - 1\right) + J_{02}\left(Exp\left(\frac{qV}{n_2 k_B T}\right) - 1\right)$$

where J_{01} is related to thermionic emission, and J_{02} is the diffusion component.

If only one of the components dominates:

$$V_{oc} = \frac{nk_B T}{q} Ln\left(\frac{J_{sc} + J_0}{J_0}\right) \approx \frac{nk_B T}{q} Ln\left(\frac{J_{sc}}{J_0}\right)$$

A linear fit (R^2 > 0.99) of a plot of V_{oc} versus ln(J_{sc}) yielded $J_0 = 1.5 \times 10^{-7}\ \mathrm{mA\ cm^{-2}}$ and a diode quality factor of n = 1.09.

An estimate of the diffusion component was obtained using:

$$J_{02} = \frac{P_n q D_p}{L_p} \approx 2.7 \times 10^{-10}\ \mathrm{mA\ cm^{-2}}$$

A doping density of N_A = 10^{17} cm^{-3}, a hole-diffusion coefficient of D_p = 8 cm^2 s^{-1},[5, 6] and a hole-diffusion length of L_p = 100 µm were used to estimate the diffusion component.

Under these conditions, $J_{02} \ll J_0$, so thermionic emission dominates.

To evaluate the thermionic emission component, the following relationship was used:

$$J_0 = \alpha A^* T^2 Exp\left(-\frac{q\phi_b}{k_B T}\right)$$

where α is the transmission coefficient; the Richardson constant, A^*, for electrons in n-Si is 120 A cm^{-2} K^{-2}; and the barrier height, ϕ_b is:

$$\phi_b = V_{fb} + V_n$$

where V_n is the difference between the potential of the Fermi level and the conduction-band-edge potential of n-Si in the bulk. The value of V_n is 0.15 V for a doping density of 10^{17} cm^{-3} at T = 298 K. $V_{fb} = 0.83 \pm 0.02$ V was determined from analysis of the Mott-Schottky data. Therefore, $\phi_b = 0.98 \pm 0.02$ V, yielding:

$$\alpha = \frac{J_0}{A^* T^2 Exp\left(-\frac{q\phi_b}{k_B T}\right)}$$

and resulting in a value of $\alpha = 1.1$ for $\phi_b = 1.00$ V, and α = 0.24 for $\phi_b = 0.96\,V$. Hence we estimate that α is on the order of unity for the system of interest.

Measurement of Faradaic efficiency for production of O_2:

To monitor the concentration of O_2 throughout the experiment, a Neofox fluorescence probe (Foxy probe, Ocean Optics) was used in an airtight cell with a side-facing quartz window. The measured concentration of O_2 was calibrated against the standard concentration of oxygen

in water (7700 μg L^{-1} or 2.4×10^{-4} M) under a standard 20.9% (by volume) oxygen atmosphere. The reference electrode was a Hg/HgO/1.0 M KOH electrode and the counter electrode was a Pt mesh (Alfa-Aesar, 100 mesh, 99.9% trace metal basis), which was placed in a fritted compartment. The cell had a volume of 43.6 mL and was purged with a stream of ultra-high purity Ar (g) for ~ 1 h before data collection. The geometric area of the working electrode was ~ 0.6 cm^2, and the current was maintained at 0.30 mA to prevent the formation of bubbles on electrode surfaces. The amount of oxygen generated versus time assuming 100% Faradaic efficiency was calculated by converting the charge passed into coulombs by multiplying the current passed (in mA·h as measured by the potentiostat) by 3.6, and then converting to units of μg O_2 by multiplying by the charge passed by 83 (because 83 is the conversion factor for 1 coulomb of electrons to micrograms of O_2).

Transmission-electron microscopy (TEM):

Samples were prepared for cross-sectional TEM using conventional polishing and milling techniques. Cross-section samples were mounted on Mo slot grids (SPI Supplies) with an M-Bond 610 adhesive. The samples were then manually polished with diamond lapping film discs (Allied High Tech Products, Inc.). The samples were further polished with a dimpling machine (E.A. Fischione Instruments, Inc.), and final thinning was performed with Ar ion milling. TEM and scanning-TEM (STEM) imaging were performed with an FEI Tecnai F30ST microscope with an accelerating voltage of 300 kV. Energy-dispersive spectroscopy (EDS) line scans were collected in STEM mode using an Oxford energy-dispersive x-ray detector.

UV-Visible absorptance measurements:

The optical absorptance of NiO_x-coated Si with a CoO_x interfacial layer (60 ALD cycles) was indirectly determined by separately measuring the total reflectance and transmittance using an Agilent Cary 5000 UV-Vis spectrometer, and subtracting the measured values from unity.

Atomic-force microscopy:

Atomic-force microscopy (AFM) was performed using a Bruker Dimension Icon operating in ScanAsyst mode with Bruker ScanAsyst-Air probes (silicon tip, silicon nitride cantilever, spring constant: 0.4 N/m, frequency: 50-90 kHz) for n-Si, n-Si/$SiO_{x,RCA}$/CoO_x and n-Si/$SiO_{x,RCA}$/CoO_x/NiO_x, and operating in KPFM-FM mode with Bruker PFQNE-AL probes (silicon tip, silicon nitride cantilever, spring constant: 0.4-1.2 N/m, frequency: 200-400 kHz) for n-Si and n-Si/CoO_x.

The scan size was 500 nm × 500 nm and 3 μm ×3 μm for the ScanAsyst and KPFM-FM modes, respectively. The images were analyzed using NanoScope Analyst software (version 1.40).

X-Ray Photoelectron Spectroscopy:

X-ray photoelectron spectroscopic (XPS) data were obtained using an AXIS Ultra DLD instrument (Kratos Analytical), at a background pressure of 1×10^{-9} Torr. High-intensity excitation was provided by monochromatic Al Kα X-rays that were 1486.6 eV in energy with a 0.2 eV resolution at full width at half-maximum. Photoelectrons were collected at the surface normal using a retarding (pass) energy of 20 eV. The peak energies were calibrated against the binding

energy of the adventitious C 1s peak, which was taken to be 284.5 eV.

Grazing incidence X-ray diffraction:

Grazing incidence X-ray diffraction analysis was performed using a Bruker D8 Discover system equipped with a 2-dimentional Vantec-500 detector. Cu-Kα radiation (1.54 Å) was generated at a tube voltage of 1 kV and a tube current of 50 mA. The incident beam was focused with a mono-capillary collimator. The incident angle was fixed at 5 degrees. A laser beam marked the focal spot on the specimen fixed on an x-y-z stage. The scattered diffraction was registered by a 2-dimensional detector with an angular resolution < 0.04 degrees, and enabled the simultaneous detection of the diffraction data in a 2theta range of 20 ~ 90 degrees. The detected radiation was counted for 2000 s to obtain an appropriate XRD profile. Data were analyzed with Bruker EVA software.

Calculations

Charge required to dissolve the CoO_x interfacial layer:

The thickness of the interfacial CoO_x layer was measured to be 2-3 nm, so 3 nm was used as the thickness in this calculation. Assuming that the mass density of the interfacial layer is 8.9 g cm^{-3} (the highest density among Co, CoO, Co_2O_3 and CoO_2), and that the interfacial layer is Co metal that is oxidized to form CoO_2 before being dissolved by 1.0 M KOH(aq), the required charge per cm^2 is:

$$\frac{3 \times 10^{-7} \times 1 \times 8.9}{58.93} \times 96500 \times 4\ \mathrm{cm}^{-2} = 0.017\ \mathrm{cm}^{-2}$$

The charge passed per cm^2 for 1700 h at 30 mA cm^{-2} is:

$$1700 \times 3600 \times 30 \times 10^{-3}\ \mathrm{C\ cm^{-2}} = 183600\ \mathrm{C\ cm^{-2}}$$

The ratio of the total charge passed to the charge required to dissolve the CoO_x was therefore:

$$\frac{183600}{0.017} \approx 1 \times 10^{7}$$

Charge density needed to dissolve the Si wafer:

The thickness of the Si wafer was 0.525 mm, and the mass density of Si is 2.3 g cm^{-3}. Assuming that the Si wafer was oxidized to form K_2SiO_3, the charge density passed would be:

$$\frac{0.525 \times 10^{-1} \times 1 \times 2.3}{28} \times 4 \times 96500\ \mathrm{cm^{-2}} = 1665\ \mathrm{C\ cm^{-2}}$$

The ratio of the total charge passed to the charge required to dissolve Si wafer is thus:

$$\frac{183600}{1665} \approx 110.$$

Calculation of solar-to O_2(g) ideal regenerative-cell conversion efficiency (η_{IRC}):

Given the *J-E* data for a photoanode (potential vs RHE), the potential axis was converted to the potential relative to $E^{0\prime}(O_2/H_2O)$ by subtracting the value of *E* versus RHE from 1.23 V. The resulting potential was then multiplied by the corresponding current at each point, and the maximum value of the product for the data was found and divided by 100 to yield the solar-to-O_2(g) ideal regenerative-cell conversion efficiency. Hence, the maximum value of (*E* vs $E^{0\prime}(O_2/H_2O)$) × *J*(at *E* vs $E^{0\prime}(O_2/H_2O)$) divided by 100 yielded the solar-to O_2(g) ideal regenerative-cell conversion efficiency.

Definition of the term "equivalent open-circuit voltages (V_{oc})"

Equivalent open-circuit voltage (V_{oc}) means the voltage required to obtain a shift in the *J-E* behavior equivalent to that observed for the photoelectrode, through a load-line analysis based on an equivalent-circuit model consisting of a photodiode connected in series with a dark electrolysis cell.

Clarification on the nonzero electrode potential vs $E^{o'}(O_2/H_2O)$) of n-Si/$SiO_{x,RCA}$/CoO_x/NiO_x photoanodes in contact with 1.0 M KOH(aq) in the dark (Figure 2A)

The nonzero electrode potential vs $E^{o'}(O_2/H_2O)$) of n-Si/$SiO_{x,RCA}$/CoO_x/NiO_x can be attributed to the cathodic redox peaks associated with NiO_x,, which intersect the potential axis (*E* axis) at a nonzero potential vs $E^{o'}(O_2/H_2O)$) in the *J-E* behavior.

Supplementary Discussion

CoO_x layers with thicknesses < 2 nm did not provide a uniform coating on the surface of the Si substrate sufficient to prevent direct contact between the Si and NiO_x. The spatially non-uniform interface therefore consisted of a mixture of low and high barrier-height contacts, and reduced the overall barrier height of the junction and reduced the photovoltage relative to devices that had thicker CoO_x layers, which provided a more uniform coating (Figure S1C). Furthermore, very thin CoO_x layers would not be expected to provide robust protection against continuous oxidation or degradation to the underlying silicon and chemical oxide layers during the high-temperature sputter-deposition of the NiO_x layer. This expectation is supported by the observed smaller slope of the J-E data near 0 mA cm^{-2} of current density (Figure S1A) for the

thinnest CoO_x films relative to the behavior observed for thicker films. Much thicker CoO_x films (> 2 nm) resulted in increased resistive losses, which decreased the performance of the photoanodes. Therefore, a CoO_x film with a thickness of 2 nm (corresponding to 60 cycles of ALD growth) was used in this work.

The behavior of CoO_x-coated Si photoanodes without a NiO_x coating was evaluated in 1.0 M KOH(aq), and exhibited a positive shift of ~ 80 mV in the photocurrent-onset potential relative to photoanodes with NiO_x coatings, consistent with to the larger overpotential of the CoO_x catalyst relative to the behavior of NiO_x (Figure S6A). Over 8 h of operation in 1.0 M KOH(aq) at a potential of 1.63 V versus RHE and under 100 mW cm^{-2} of simulated solar illumination, a positive shift of ~200 mV in the photocurrent-onset potential of n-$Si/SiO_{x,RCA}/CoO_x$ was observed, suggesting degradation of the junction, possibly caused by the conversion of the CoO_x layer to ion-permeable $Co(OH)_2$/CoOOH which would allow the continuous passivation of the underlying Si and would result in a decreased current density over time (Figure S6A, B). For comparison, a positive shift of the photocurrent-onset potential was not observed for an n-$Si/SiO_{x,RCA}/CoO_x/NiO_x$ photoelectrode after 20 h of continuous operation in 1.0 M KOH(aq) under the same conditions (Figure S6A). However, a degradation of photoresponse was observed for n-$Si/SiO_{x,RCA}/CoO_x/NiO_x$ photoelectrodes over 1700 h of operation which could, in principle, be related to slow electrochemical conversion of CoO_x to $Co(OH)_2$ and then to ion-permeable CoOOH. The rate of such conversion, however, might be minimized further with improved control over the NiO_x processing conditions.

Supplementary Figures:

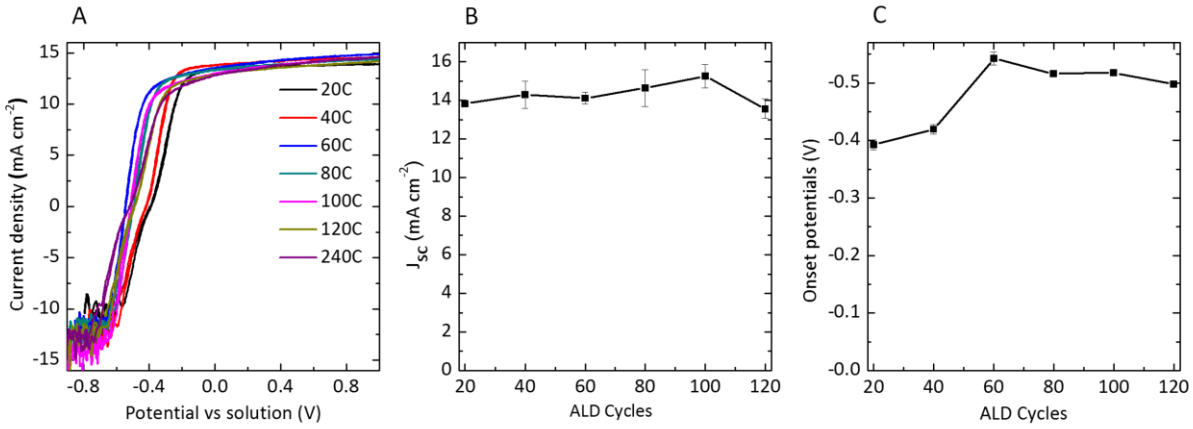

Figure S1. (A) *J-E* behavior of n-Si/$SiO_{x,RCA}$/CoO_x/NiO_x photoanodes as a function of the thickness of the CoO_x interfacial layer, ranging from 20 ALD cycles (20C) to 240 ALD cycles (240C), under 0.4-Sun simulated solar illumination in a solution of 0.35 M $K_4Fe(CN)_6$, 0.05 M $K_3Fe(CN)_6$ and 1.0 M KCl (aq). (B, C) Dependence of the photoelectrochemical behavior of n-Si/$SiO_{x,RCA}$/CoO_x/NiO_x photoanodes under 40 mW cm^{-2} of simulated solar illumination and in contact with 0.35 M $K_4Fe(CN)_6$, 0.05 M $K_3Fe(CN)_6$ and 1.0 M KCl(aq). (B) Light-limited current density and (C) Photocurrent-onset potentials relative to the solution potential $E(Fe(CN)_6^{3-/4-})$ (Onset potentials for short) versus the CoO_x layer thickness as indicated by the number of ALD cycles used to deposit the coating.

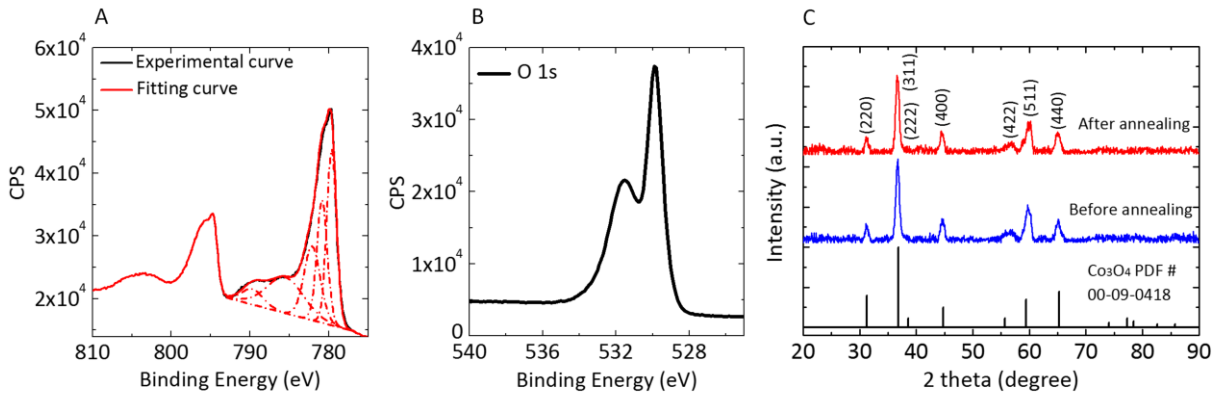

Figure S2. (A, B) X-Ray photoelectron spectra (XPS) for an n-Si/$SiO_{x,RCA}$/CoO_x photoelectrode. The binding energies used for fitting of the Co $2p_{3/2}$ peaks were 779.6 eV, 780.8 eV, 782.2 eV, 785.5 eV, 789.7 eV. (C) Grazing incidence X-ray diffraction (GIXRD) pattern for a CoO_x film (1000 ALD cycles) on an n-Si/$SiO_{x,RCA}$ substrate before and after annealing in an AJA high-vacuum magnetron sputtering chamber at 300 ℃ under the sputtering gas environment.

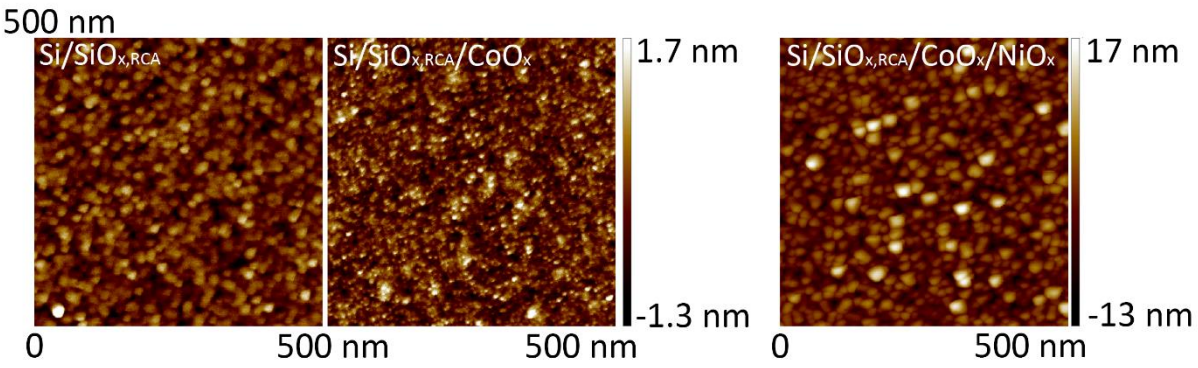

Figure S3. AFM images showing the surface morphology of n-Si/$SiO_{x,RCA}$, n-Si/$SiO_{x,RCA}$/CoO_x, and n-Si/$SiO_{x,RCA}$/CoO_x/NiO_x, respectively.

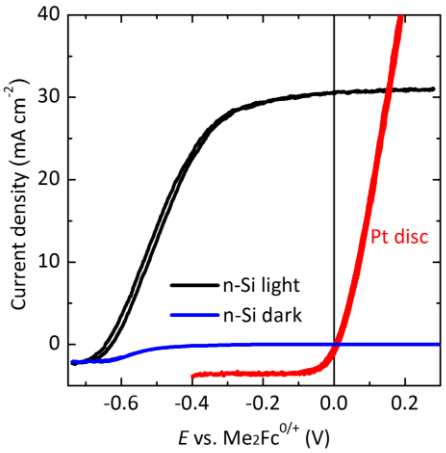

Figure S4. *J-E* behavior of a freshly etched n-Si photoanode in contact with 0.20 M Me_2Fc/0.010 M Me_2Fc^+ in CH_3OH with 1.5 M $LiClO_4$ added as a supporting electrolyte and under 100 mW cm^{-2} of ELH-type W-halogen illumination (black) and in the dark (blue).

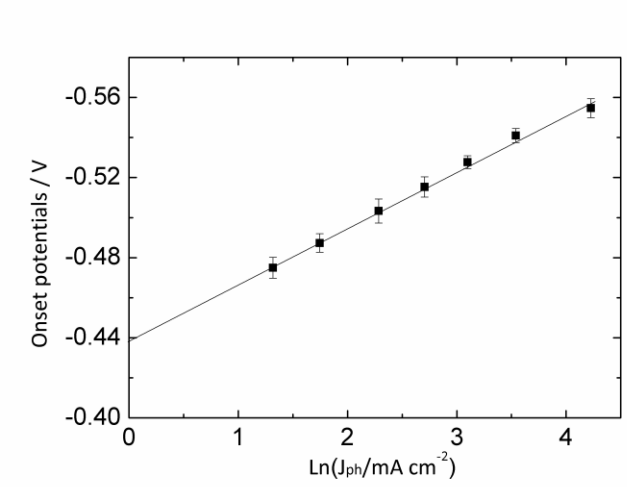

Figure S5. Photocurrent-onset potentials relative to $E(Fe(CN)_6^{3-/4-})$ (Onset potentials for short) for an n-Si/$SiO_{x,RCA}$/CoO_x/NiO_x photoanode in contact with a solution of 0.35 M $K_4Fe(CN)_6$, 0.05 M $K_3Fe(CN)_6$ and 1.0 M KCl(aq) under 200 mW cm^{-2}, 100 mW cm^{-2}, 63 mW cm^{-2}, 40 mW cm^{-2},25 mW cm^{-2},16 mW cm^{-2}and 10 mW cm^{-2} of AM 1.5G simulated illumination from a Xe lamp. Neutral density filters were used to attenuate the light intensity to produce the desired

illumination levels at the sample surface.

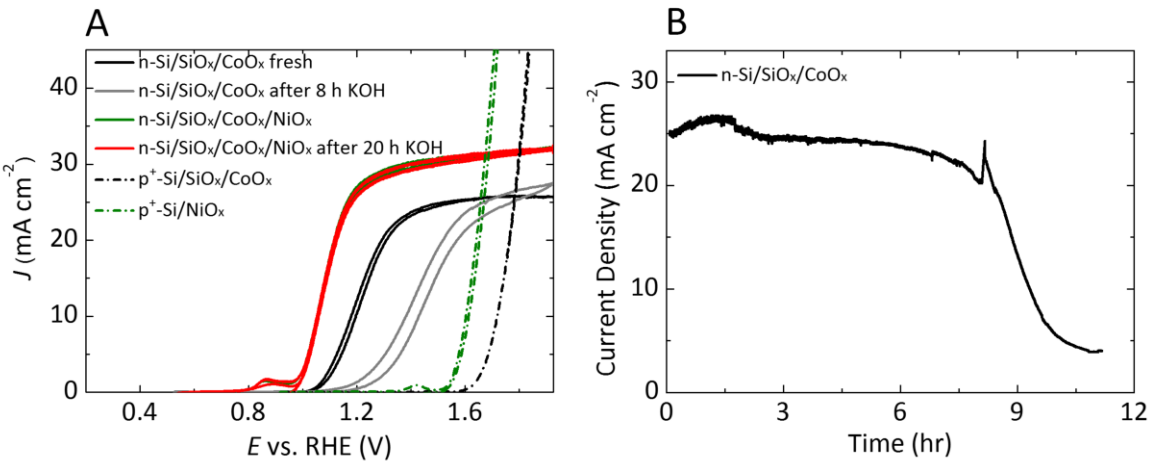

Figure S6. (A) Representative current-density versus potential (J-E) behavior of n-Si/$SiO_{x,RCA}$/CoO_x and n-Si/$SiO_{x,RCA}$/CoO_x/NiO_x photoanodes in contact with 1.0 M KOH(aq) under 100 mW cm^{-2} of AM 1.5G simulated solar illumination before and after 8 h and 20 h of continuous operation at 1.63 V vs RHE, respectively. The J-E behavior of p^+-Si/$SiO_{x,RCA}$/CoO_x and p^+-Si/NiO_x is also shown. (B) Chronoamperometry of an n-Si/$SiO_{x,RCA}$/CoO_x photoanode biased at 1.63 V vs RHE under 100 mW cm^{-2} of simulated 1.5 G solar illumination from an ENH-type tungsten-halogen lamp.

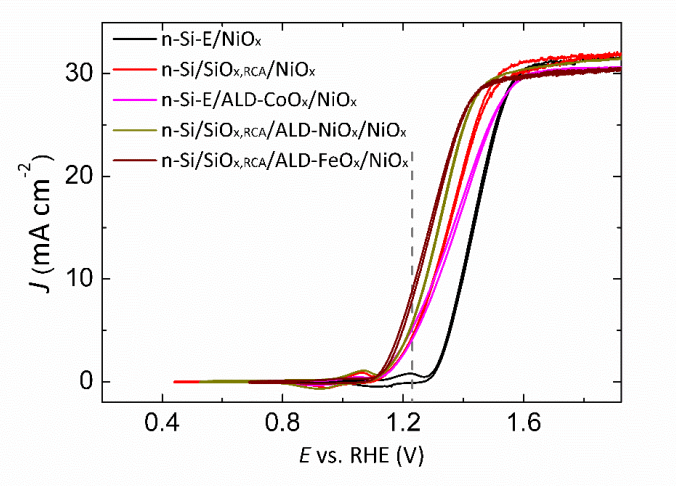

Figure S7. Representative *J-E* data for photoanodes in 1.0 M KOH(aq) under 100 mW cm^{-2} of simulated AM1.5G solar illumination. n-Si-E indicates that the n-Si was freshly etched in buffered HF(aq) before the next processing step. $SiO_{x,RCA}$ indicates that the RCA SC-2 etching procedure generated SiO_x. A nominally identical reactive RF sputtering process was used to deposit the multifunctional NiO_x layer onto each of these electrodes.

References

1. H. B. Gray, D. N. Hendrickson and Y. S. Sohn, *Inorg. Chem.*, 1971, **10**, 1559-1563.
2. K. Sun, Y. Kuang, E. A. Verlage, B. S. Brunschwig, C. W. Tu and N. S. Lewis, *Adv. Energy Mater.*, 2015, DOI: 10.1002/aenm.201402276.
3. K. Sun, F. H. Saadi, M. Lichterman, W. G. Hale, H.-P. Wang, X. Zhou, N. T. Plymale, S. Omelchenko, J.-H. He, K. M. Papadantonakis, B. S. Brunschwig and N. S. Lewis, *Proc. Natl. Acad. Sci. U.S.A.*, 2015, **112**, 3612-3617.
4. K. Sun, M. T. McDowell, A. C. Nielander, S. Hu, M. R. Shaner, F. Yang, B. S. Brunschwig and N. S. Lewis, *J. Phys. Chem. Lett.*, 2015, **6**, 592-598.
5. C. H. Wang, K. Misiakos and A. Neugroschel, *IEEE Trans. Electron. Devices*, 1990, **37**, 1314-1322.
6. W. R. Thurber, R. L. Mattis and Y. M. Liu, *The Relationship between resistivity and dopant density for phosphorus- and boron-doped silicon*, U.S. Dept. of Commerce, National Bureau of Standards, 1981.